Dalton Transactions

ROYAL SOCIETY OF CHEMISTRY

PAPER

View Article Online
View Journal | View Issue

Cite this: *Dalton Trans.*, 2020, **49**, 1891

Facile synthesis of tellurium nano- and microstructures by trace HCl in ionic liquids†

Tao Zhang,[a,b] Thomas Doert, [a] Kai Schwedtmann,[a] Jan J. Weigand [a] and Michael Ruck *[a,c]

Received 2nd December 2019,
Accepted 13th January 2020

DOI: 10.1039/c9dt04604f

rsc.li/dalton

Ionic liquids (ILs) are widely used as versatile solvents for the synthesis of nanomaterials. However, the effect of IL impurities on the formation of nanomaterials is often neglected. Herein, we report on the formation of tellurium (Te) nanoparticles from the reaction of trialkylphosphane tellurides, formed by reactive dissolution of Te in dried commercial trihexyltetradecylphosphonium chloride ($[P_{66614}]Cl$) at high temperatures, with common polar protic solvents (*e.g.* water, alcohols, or amides). Highly homogeneous Te nano- and microstructures with various sizes and morphologies including three-dimensional (3D) Te fusiform assemblies and 3D aloe-like Te microarchitectures are obtained. Our investigation shows that trace amounts of HCl impurities in $[P_{66614}]Cl$ tend to remain as $[P_{66614}][HCl_2]$ due to the strong interaction with Cl^-. The addition of a polar, protic solvent liberates active HCl from the HCl_2^- anion which we found to play an essential role in the formation of Te particles due to the accelerating effect of P–Te bond cleavage. This approach presents a general and convenient synthetic strategy for the preparation of Te nano- and microstructures.

1. Introduction

Ionic liquids (ILs) are, by definition, a family of molten salts with melting points below 100 °C.[1] In the past few decades, ILs have become alternative solvents to traditional organic solvents and brought a revolution in both academic and industrial areas including catalysis, separation, organic synthesis, and material sciences.[2–7] The unique properties such as excellent thermal stability, low vapor pressure, wide liquid range and electrochemical window, and tunable solvent properties are certainly the most highlighted and well-studied advantages of ILs in literature and the reasons for their broad application.[8–12]

Toxicity, chemical reactivity, and impurity of ILs are rarely reported,[13–15] and are typically considered as negative aspects of ILs. For instance, impurities in ILs may significantly influence their chemical and physical properties, which may cause non-uniform experimental data. Some examples: Suranna and co-workers reported that the presence of halide impurities in 1-butyl-3-methylimidazolium tetrafluoroborate ($[BMIm][BF_4]$) has a detrimental effect on the activity of organometallic catalysts towards Michael additions.[16] Brutchey and co-workers demonstrated that trace amounts of water, chloride, and 1-methylimidazole in $[BMIm][BF_4]$ cause polydisperse and irregularly shaped ensembles of silver nanoparticles, and also negatively influence the stabilization of the resulting particles.[15]

On the other hand, impurities of ILs can play a positive role in reactions. We previously showed that HCl impurity in $[P_{66614}]Cl$ leads to a surface activation of elemental copper, promoting the formation of $Cu_{3-x}P$ with a high product yield.[17] Another investigation revealed that trace amounts of metal ion impurities in 1-ethyl-3-methylimidazolium chloride ([EMIm]Cl), particularly Cu and Cr ions, promote reactions of cellulose depolymerization drastically due to the significant synergistic effect of metal halides and ILs.[18,19] This stimulated us to continue exploring cases in which trace impurities commonly found in ILs have positive impacts on reactions.

Elemental tellurium (Te) is a typical p-type semiconductor with a narrow band gap (0.35 eV) at room temperature, exhibiting attractive physical and chemical properties with potential applications in a variety of different areas such as gas sensing, ion detection and removal, photoconductivity, and lithium–tellurium batteries.[20–24] Te nano- and microstructures are commonly synthesized using solution-based strategies, typically by direct reduction of a Te precursor (*e.g.* a tellurite or tellurate) in the presence of a surfactant like polyvinylpyrrolidone

[a]*Faculty of Chemistry and Food Chemistry, Technische Universität Dresden, 01062 Dresden, Germany. E-mail: michael.ruck@tu-dresden.de*
[b]*Beijing Key Laboratory of Ionic Liquids Clean Process, CAS Key Laboratory of Green Process and Engineering, Institute of Process Engineering, Chinese Academy of Sciences, 100190 Beijing, China*
[c]*Max Planck Institute for Chemical Physics of Solids, 01187 Dresden, Germany*
†Electronic supplementary information (ESI) available. See DOI: 10.1039/c9dt04604f

(PVP).[25–27] Hence, the reaction systems become complicated. In the present work, we developed a new and convenient synthetic method for the creation of novel, complex 3D Te microstructures by exploiting the reaction of trialkylphosphane tellurides, formed by reactive dissolution of Te in dried $[P_{66614}]Cl$ at high temperatures, with polar protic solvents. The reaction can be triggered by the amount of HCl in $[P_{66614}]Cl$. According to our scanning electron microscopy (SEM) investigations, the sizes and morphologies of Te particles can be tuned by varying the polar protic solvents.

2. Experimental

2.1. Chemicals

Trihexyltetradecylphosphonium chloride ($[P_{66614}]Cl$, >95%), trihexyltetradecylphosphonium dicyanamide ($[P_{66614}][N(CN)_2]$, >95%), and trihexyltetradecylphosphonium decanoate ($[P_{66614}]$[decanoate], >95%) were purchased from io-li-tec, Germany. Te powder (Te, −325 mesh, 99.99%) was purchased from ABCR GmbH, Germany. All the organic solvents were purchased from Sigma-Aldrich. The typical drying of ILs was performed under dynamic vacuum at 110 °C overnight. The HCl impurity in commercial $[P_{66614}]Cl$ was removed by neutralization with a sodium hydroxide solution, as previously described.[17] The Te powder was reduced in an H_2 atmosphere at 400 °C for 7 h. All other chemicals were used as received without further purification.

2.2. Preparation of Te solution in $[P_{66614}]Cl$, $[P_{66614}][N(CN)_2]$, and $[P_{66614}]$[decanoate]

The Te solution in ILs was prepared according to our previously reported method.[14] Taking Te solution in $[P_{66614}]Cl$ as an example, 12 mg Te powder was added to 4 g $[P_{66614}]Cl$ in an Ar-filled glovebox. The mixture was transferred into a 25 mL Teflon lined stainless steel autoclave in the glovebox. The autoclave was sealed, taken out of the glovebox, and then placed in an oven at 250 °C for 48 h. After the autoclave was cooled down to room temperature, a clear, light yellow Te solution was obtained as the unsaturated Te solution. If more Te powder (*e.g.* 20 or 24 mg) was used in the dissolution test, some undissolved Te powder was observed. The saturated Te solution was obtained by removal of the undissolved Te powder.

2.3. General synthesis of Te nano- and microstructures using protic solvents

Taking ethanol as an example, typically, 0.5 mL Te solution in $[P_{66614}]Cl$ was placed in a 5 mL screw-cap glass bottle. Then 2 mL ethanol was added to the bottle immediately. The mixture was shaken strongly until a permanent black precipitate formed. Normally, this process needs less than one minute. The precipitate was separated by centrifugation, washed with acetone or toluene first and then with ethanol for several times. For water and ethylene glycol, a longer time is required to achieve Te precipitation.

2.4. Materials characterization

Powder X-ray diffraction (PXRD) patterns were typically recorded using a PANalytical X'Pert Pro diffractometer with Cu-$K_\alpha 1$ radiation (λ = 154.0562 pm). The scanning electron microscopy (SEM) images were obtained at 3 kV using a Hitachi SU8020 field emission SEM coupled with energy-dispersive X-ray spectroscopy (EDX; Oxford X-Max^N). NMR spectra were measured on a Bruker AVANCE III HDX, 500 MHz Ascend (^{31}P (202.45 MHz); ^{125}Te (157.78 MHz)) equipped with a Prodigy-Cryo Probe. Chemical shifts were referenced to $\delta_{H_3PO_4(85\%)}$ = 0.00 ppm (31P) and δ_{Me_2Te} = 0.00 ppm (^{125}Te). Chemical shifts (δ) are reported in ppm. Coupling constants (J) are reported in Hz.

3. Results and discussion

The phosphonium IL $[P_{66614}]Cl$ was dried at 110 °C overnight under dynamic vacuum prior to use. The trialkylphosphane tellurides were prepared by dissolving Te in $[P_{66614}]Cl$ at high temperatures according to our previous report.[14] For convenience, the trialkylphosphane tellurides obtained by dissolving Te in $[P_{66614}]Cl$ are defined here as "Te solution in $[P_{66614}]Cl$". In order to obtain Te nano- and microstructures, various solvents were tested (Table S1;† see Experimental section for more details). Both non-polar solvents (*e.g. n*-hexane, toluene, chloroform, or diethyl ether) and polar aprotic solvents (*e.g.* tetrahydrofuran, ethyl acetate, acetone, dimethylformamide, acetonitrile, or dimethyl sulfoxide) are miscible with trialkylphosphane tellurides in $[P_{66614}]Cl$ without Te precipitation, whereas polar protic solvents (*e.g.* water, alcohols, amides, or carboxylic acids) cause Te precipitation with a variety of sizes and morphologies of the obtained Te particles.

3.1. Synthesis of Te nano- and microstructures using alcohols

The precipitation of Te powder from Te solutions in $[P_{66614}]Cl$ depends slightly on the alkyl chain length of the applied monohydric alcohol (see Experimental section for more details). Ethanol can cause precipitation within a few seconds by mixing it with Te solution in $[P_{66614}]Cl$. With increasing alkyl chain length of the alcohols (*n*-butanol, *n*-hexanol, *n*-octanol, and *n*-decanol), the precipitation of Te powder took a verifiably longer time but not more than one minute. The precipitates were identified as crystalline Te by powder X-ray diffraction (PXRD; Fig. 1) and energy-dispersive X-ray spectroscopy (EDX; Fig. S1†). All reflections can be indexed with the trigonal unit cell of Te in space group $P3_121$ (ICSD no. 76150).[28] The SEM images (Fig. 2a–e) display that all obtained Te particles have quite homogeneous fusiform morphologies with lengths of 300–400 nm. With increasing alkyl chain length of the alcohols, these Te fusiforms maintain similar sizes and shapes but their edges become slightly sharper. The high-magnification SEM image (Fig. 2f) clearly reveals that a single Te fusiform is composed of even smaller Te nanofusi-

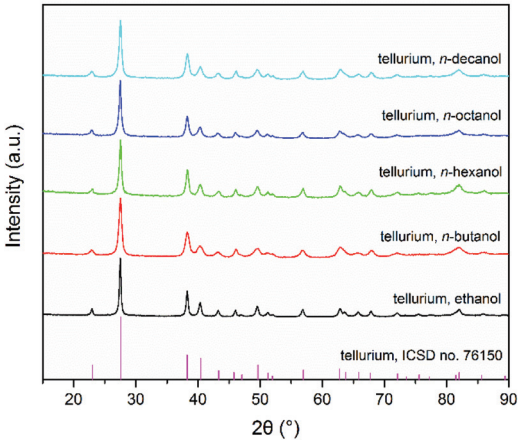

Fig. 1 PXRD patterns (Cu-Kα_1) of Te powders obtained by mixing monohydric alcohols with Te solution in [P_{66614}]Cl.

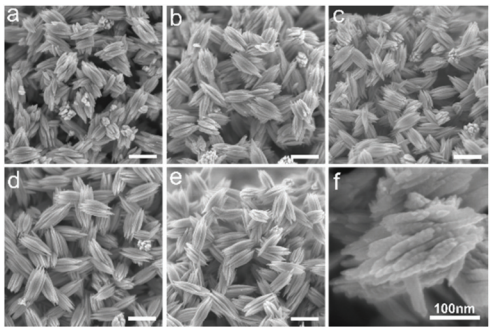

Fig. 2 SEM images of Te particles obtained by mixing Te solution in [P_{66614}]Cl with ethanol (a), *n*-butanol (b), *n*-hexanol (c), *n*-octanol (d), or *n*-decanol (e) (scale bar, a–e, 300 nm). SEM image of a single 3D microfusiform particle obtained in *n*-butanol (f).

forms with lengths of 50–400 nm, *i.e.* Te nanofusiform assemblies form a Te microfusiform.

The mixture of 2 mL ethylene glycol and 0.5 mL Te solution in [P_{66614}]Cl turned out to be immiscible. Nonetheless, when these two phases were placed statically under air for several hours, a dark precipitate was observed in the upper IL phase (Fig. S2a†). The formation of crystalline Te was confirmed by PXRD. The SEM images are shown in Fig. 3. The low-magnification SEM image (Fig. 3a) demonstrates the overall mor-

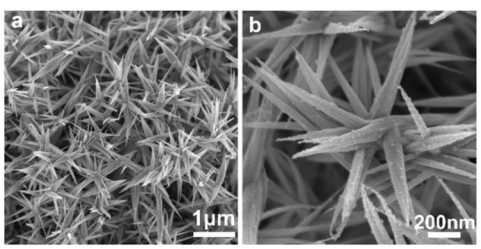

Fig. 3 SEM images of obtained Te particles using ethylene glycol as the protic solvent.

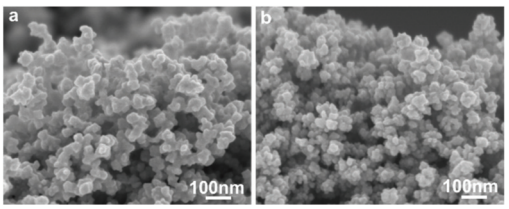

Fig. 4 SEM images of obtained Te nanoparticles using allyl alcohol (a) or propargyl alcohol (b) as the protic solvent.

phology of aloe-like Te microstructures with a diameter of approximately 1.3 μm. The high-magnification SEM image in Fig. 3b shows that these microstructures are assemblies of lancets with typical lengths of about 600 nm in various directions. The rough surfaces of these lancets are clearly visible in Fig. 3b.

As shown in Fig. 4, polyhedral nanoparticles of crystalline Te (as evidenced by PXRD) with diameters of about 50 nm were synthesized in the presence of allyl alcohol or propargyl alcohol as examples of unsaturated alcohols.

3.2. Synthesis of Te microstructures using amides

Protic amides, such as formamide and *N*-methylformamide, also lead to the formation of crystalline Te powders according to PXRD. Fig. 5a and b show the corresponding SEM images obtained from formamide, displaying also the formation of fusiform assemblies. However, the sizes with lengths of about 100 nm are much smaller than those obtained from monohydric alcohols.

In contrast, Te particles obtained from *N*-methylformamide (Fig. 5c and d) show aggregates of intergrown elongated particles with diameters of approximately 400–600 nm (Fig. 5c). The magnified image reveals that each of these Te particles consists of much smaller, intergrown nanoparticles (Fig. 5d).

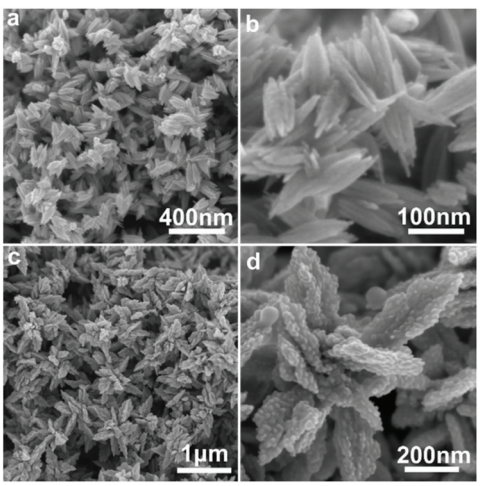

Fig. 5 SEM images of obtained Te particles using formamide (a, b) or *N*-methylformamide (c, d) as the protic solvent.

3.3. Synthesis of Te nanostructures using carboxylic acids

Carboxylic acids, such as formic acid, acetic acid, and propionic acid, lead quite rapidly to the precipitation of Te particles when mixed with Te solution in $[P_{66614}]Cl$. SEM images reveal the formation of Te nanoparticles with a size of 30–50 nm, without creating complex 3D Te architectures (Fig. S3†).

3.4. Synthesis of Te microstructures using water

Water, as one of the most widely used solvents, also leads to the formation of Te microstructures. Similar to ethylene glycol, 2 mL water added to a 0.5 mL Te solution in $[P_{66614}]Cl$ shows immiscibility. A dark Te precipitate formed in the upper IL phase (Fig. S2b†) when the water and Te solution phases were placed statically overnight. The formed Te precipitate consists of fusiform assemblies with typical lengths of about 4 μm, which are much larger than those obtained from monohydric alcohols (SEM image in Fig. S4†).

3.5. Possible formation mechanism

As previously reported by us, relatively high amounts of Te powder can be dissolved in certain phosphonium-based ILs, such as trihexyltetradecylphosphonium dicyanamide ($[P_{66614}][N(CN)_2]$), trihexyltetradecylphosphonium decanoate ($[P_{66614}]$[decanoate]), and tetrabutylphosphonium decanoate ($[P_{4444}]$[decanoate]).[14] NMR investigations show that the quaternary phosphonium cations undergo an S_N2-type reaction to the respective trialkylphosphane telluride *via* the elimination of one of the alkyl chains. This process takes place at relatively high temperatures in the presence of Te and leads to its dissolution in the phosphonium-based ILs. In the case of $[P_{66614}]Cl$, however, a very limited Te solubility was observed for both saturated and unsaturated Te solutions (for details see Experimental section) indicated by the absence of the respective resonances in the ^{125}Te NMR spectra due to the very low concentration of dissolved Te-based species. In order to increase the concentration and to obtain meaningful ^{125}Te NMR spectra, for both cases, the excess of $[P_{66614}]Cl$ was removed *via* flash chromatography and the resulted solutions are accordingly denoted as Te_{sat} and Te_{unsat}.

The ^{31}P NMR spectrum in Fig. 6b for Te_{sat} indicates an upfield shifted resonance at $\delta(^{31}P) = -13.6$ ppm compared to that of the pure $[P_{66614}]Cl$ ($\delta(^{31}P) = 33.2$ ppm).[29] The large $^1J_{PTe}$ coupling constant of 1665 Hz is in the range of typical phosphane tellurides.[30] The corresponding ^{125}Te NMR spectrum (Fig. 6d) shows one doublet resonance at $\delta(^{125}Te) = -778.8$ ppm with the same coupling constant $^1J_{TeP} = 1665$ Hz. Both ^{31}P and ^{125}Te NMR spectra evidence a P–Te bond formation and the formation of trialkylphosphane tellurides. For Te_{unsat}, however, the corresponding ^{31}P and ^{125}Te NMR spectra (Fig. 6a and c) show only one single resonance ($\delta(^{31}P) = -22.7$ ppm, and $\delta(^{125}Te) = -781.7$ ppm), respectively. The spectra variations between Te_{sat} and Te_{unsat} indicate that a rapid exchange between the free phosphane and phosphane tellurides happens, reaching a dynamic equilibrium. Based on the above investigations, we can conclude that trialkylphosphane tellurides form according to the reaction of $[P_{66614}]Cl$ with elemental Te *via* nucleophilic attack of Cl^- at a relatively high temperature, which are well comparable with those of Te solution in $[P_{66614}][N(CN)_2]$ and $[P_{66614}]$[decanoate].[14]

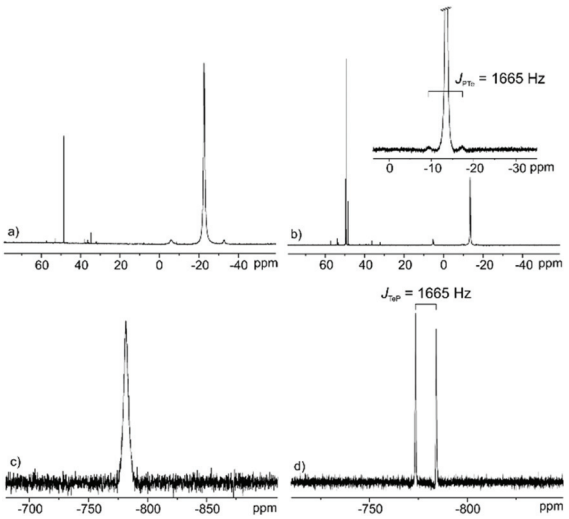

Fig. 6 ^{31}P NMR spectra of Te_{unsat} (a) and Te_{sat} (b) as well as ^{125}Te NMR spectra of Te_{unsat} (c) and Te_{sat} (d) solution in $[P_{66614}]Cl$ after removal of excess of ILs *via* flash chromatography.

The Te solution in $[P_{66614}][N(CN)_2]$ or $[P_{66614}]$[decanoate] was also tested for the Te precipitation reactions with an alcohol, but no precipitates were observed (Fig. S5†). This finding indicates that the Te precipitation reaction seems to only happen in the chloride system (*e.g.* $[P_{66614}]Cl$). It is well known that commercially available $[P_{66614}]Cl$ usually contains around 0.1–0.5% HCl as a result of its preparation,[17,31] and this impurity is difficult to remove using standard Schlenk line technique. From our findings, we can conclude that the presence of HCl impurities in $[P_{66614}]Cl$ decreased the solubility of Te (Fig. S6†). Although the presence of HCl impurity seems to reduce the solubility of Te in $[P_{66614}]Cl$, it plays at the same time an essential role in the formation of Te microstructures after the addition of polar protic solvents. We verified this hypothesis by the neutralization of commercially available $[P_{66614}]Cl$ with sodium hydroxide solution to remove all HCl impurities and subsequently extensive drying on the Schlenk line. The neutralized and dried $[P_{66614}]Cl$ failed to form Te precipitation when contacted with alcohols (*e.g.* ethanol). However, when alcohols were replaced by carboxylic acids (*e.g.* acetic acid) to mix with the purified Te solution in $[P_{66614}]Cl$, a very fast precipitation occurred and was identified to be crystalline Te by PXRD.

Based on our findings, we believe that (A) the trialkylphosphane tellurides formation with Te dissolving in $[P_{66614}]Cl$ and (B) the appropriate acidity combination from both HCl impurity and polar protic solvents are crucial for the formation of Te particles. The acidity of the added carboxylic acids is strong enough for a rapid P–Te bond cleavage, either in the presence or absence of HCl impurity in $[P_{66614}]Cl$, resulting in

the Te nanoparticles precipitation. In contrast, if protic solvents (*e.g.* water, alcohols, or amides) that possess a much lower pK_a value compared to our tested acids, the HCl in $[P_{66614}]Cl$ turns out to be vital for 3D complex Te microstructures formation.

Morris and co-workers pointed out the so-called water deactivation effect in ILs, which at low concentrations the water is significantly deactivated through strong interaction with the anions of ILs, and exists as isolated single molecules or as small cluster assemblies.[32,33] Similarly, trace amounts of HCl in $[P_{66614}]Cl$ are coordinated with chloride ions to form HCl_2^- anions as previously reported (eqn (1)).[34]

$$Cl^- + HCl \rightleftharpoons HCl_2^- \quad (1)$$

The addition of protic solvents to the mixture of $[P_{66614}]Cl$/$[P_{66614}][HCl_2]$ liberates HCl, which leads to an increase in acidity and an accelerated cleavage of P–Te bonds. The morphologies and sizes of obtained Te particles are reproducible independent of the batches of commercial $[P_{66614}]Cl$ with slightly varying HCl concentration.

4. Conclusions

In summary, a variety of Te nano- and microstructures including 3D fusiform assemblies, 3D aloe-like architectures, and nanoparticles are obtained based on a convenient synthesis *via* the reaction of HCl containing Te solution in $[P_{66614}]Cl$ with polar protic solvents. Studies demonstrate that trace amount of HCl impurities in $[P_{66614}]Cl$ affects the formation of Te nano- and microstructures. Low concentration of HCl in $[P_{66614}]Cl$ tends to be deactivated through strong interaction with chloride ions to form HCl_2^- anions. The addition of protic solvents liberates HCl from the HCl_2^- anion which prompts P–Te bond cleavage and formation of Te particles.

Currently, most reports of nanoparticles preparation in ILs do not include a careful analysis of their impurities. Considering that the impurities in ILs may affect the quality of nanoparticles, they should not be underestimated. The present investigation shows that trace impurities in ILs can be utilized as a tool to establish new strategies for inorganic material synthesis. However, the impact of IL impurities on the particles formation needs to be well understood.

Conflicts of interest

There are no conflicts to declare

Acknowledgements

We would like to thank Dr Tian-Yi Li (IAPP, TU Dresden) for the help of removing excess $[P_{66614}]Cl$ in Te_{unsat} and Te_{sat} solution using flash chromatography. T. Z. acknowledges the support from China Scholarship Council (CSC No. 201404910507). This work was financially supported by the Deutsche Forschungsgemeinschaft (DFG) within the Priority Program SPP 1708.

Notes and references

1 P. Walden, *Bull. Acad. Imp. Sci. St.-Petersbourg*, 1914, **8**, 405–422.
2 V. I. Parvulescu and C. Hardacre, *Chem. Rev.*, 2007, **107**, 2615–2665.
3 M. Watanabe, M. L. Thomas, S. Zhang, K. Ueno, T. Yasuda and K. Dokko, *Chem. Rev.*, 2017, **117**, 7190–7239.
4 S. P. M. Ventura, F. A. e Silva, M. V. Quental, D. Mondal, M. G. Freire and J. A. P. Coutinho, *Chem. Rev.*, 2017, **117**, 6984–7052.
5 M. Smiglak, J. M. Pringle, X. Lu, L. Han, S. Zhang, H. Gao, D. R. MacFarlane and R. D. Rogers, *Chem. Commun.*, 2014, **50**, 9228–9250.
6 Q. Zhang and J. N. M. Shreeve, *Chem. Rev.*, 2014, **114**, 10527–10574.
7 D. R. MacFarlane, N. Tachikawa, M. Forsyth, J. M. Pringle, P. C. Howlett, G. D. Elliott, J. H. Davis, M. Watanabe, P. Simon and C. A. Angell, *Energy Environ. Sci.*, 2014, **7**, 232–250.
8 M.-R. Gao, J. Yuan and M. Antonietti, *Chem. – Eur. J.*, 2017, **23**, 5391–5403.
9 T. Welton, *Coord. Chem. Rev.*, 2004, **248**, 2459–2477.
10 G. Gebresilassie Eshetu, M. Armand, B. Scrosati and S. Passerini, *Angew. Chem., Int. Ed.*, 2014, **53**, 13342–13359.
11 D. R. MacFarlane, M. Forsyth, P. C. Howlett, M. Kar, S. Passerini, J. M. Pringle, H. Ohno, M. Watanabe, F. Yan, W. Zheng, S. Zhang and J. Zhang, *Nat. Rev. Mater.*, 2016, **1**, 15005.
12 P. Zhang, T. Wu and B. Han, *Adv. Mater.*, 2014, **26**, 6810–6827.
13 B. Kudłak, K. Owczarek and J. Namieśnik, *Environ. Sci. Pollut. Res.*, 2015, **22**, 11975–11992.
14 T. Zhang, K. Schwedtmann, J. J. Weigand, T. Doert and M. Ruck, *Chem. – Eur. J.*, 2018, **24**, 9325–9332.
15 L. L. Lazarus, C. T. Riche, N. Malmstadt and R. L. Brutchey, *Langmuir*, 2012, **28**, 15987–15993.
16 V. Gallo, P. Mastrorilli, C. F. Nobile, G. Romanazzi and G. P. Suranna, *J. Chem. Soc., Dalton Trans.*, 2002, 4339–4342.
17 M. Le Anh, A. Wolff, M. Kaiser, S. Yogendra, J. J. Weigand, J. Pallmann, E. Brunner, M. Ruck and T. Doert, *Dalton Trans.*, 2017, **46**, 15004–15011.
18 H. Zhao, H. M. Brown, J. E. Holladay and Z. C. Zhang, *Top. Catal.*, 2012, **55**, 33–37.
19 Y. Su, H. M. Brown, X. Huang, X.-D. Zhou, J. E. Amonette and Z. C. Zhang, *Appl. Catal., A*, 2009, **361**, 117–122.
20 D. Tsiulyanu, S. Marian and H. D. Liess, *Sens. Actuators, B*, 2002, **85**, 232–238.
21 Y. Wang, Z. Tang, P. Podsiadlo, Y. Elkasabi, J. Lahann and N. A. Kotov, *Adv. Mater.*, 2006, **18**, 518–522.

22 T.-Y. Wei, H.-Y. Chang and C.-C. Huang, *RSC Adv.*, 2013, **3**, 13983–13989.
23 J. He, Y. Chen, W. Lv, K. Wen, Z. Wang, W. Zhang, Y. Li, W. Qin and W. He, *ACS Nano*, 2016, **10**, 8837–8842.
24 Z. He, Y. Yang, J.-W. Liu and S.-H. Yu, *Chem. Soc. Rev.*, 2017, **46**, 2732–2753.
25 J.-W. Liu, J. Xu, W. Hu, J.-L. Yang and S.-H. Yu, *ChemNanoMat*, 2016, **2**, 167–170.
26 H. Zhu, H. Zhang, J. Liang, G. Rao, J. Li, G. Liu, Z. Du, H. Fan and J. Luo, *J. Phys. Chem. C*, 2011, **115**, 6375–6380.
27 X. Wu, Y. Wang, S. Zhou, X. Y. Yuan, T. Gao, K. Wang, S. Lou, Y. Liu and X. Shi, *Cryst. Growth Des.*, 2013, **13**, 136–142.
28 *Inorganic Crystal Structure Database, ICSD, Version 2019/1*, FIZ Karlsruhe, Germany and NIST, Gaithersburg, USA, 2019.
29 T. Zhang, K. Schwedtmann, J. J. Weigand, T. Doert and M. Ruck, *Chem. Commun.*, 2017, **53**, 7588–7591.
30 A. Nordheider, J. D. Woollins and T. Chivers, *Chem. Rev.*, 2015, **115**, 10378–10406.
31 C. J. Bradaric, A. Downard, C. Kennedy, A. J. Robertson and Y. Zhou, *Green Chem.*, 2003, **5**, 143–152.
32 R. E. Morris, *Chem. Commun.*, 2009, 2990–2998.
33 E. R. Parnham and R. E. Morris, *Acc. Chem. Res.*, 2007, **40**, 1005–1013.
34 R. Kohle, W. Kuchen and W. Peters, *Z. Anorg. Allg. Chem.*, 1987, **551**, 179–190.